JOURNAL OF Applied Polymer SCIENCE

# Preparation and Properties of Polystyrene–γ-Methacryloxypropyl Trimethoxy Silane Copolymer/Zirconia Nanohybrid Materials

**Mingkang Tong, Juan Yu, Jianzhi Song, Rongrong Qi**
School of Chemistry and Chemical Engineering, Shanghai Jiao Tong University, Dongchuan Road 800, Shanghai 200240, China
Correspondence to: R. Qi (E-mail: rrqi@sjtu.edu.cn)

**ABSTRACT:** Polystyrene (PS)–γ-methacryloxypropyl trimethoxy silane (MPTMS) copolymer/zirconia ($ZrO_2$) nanohybrid materials were successfully prepared by the combination of solvothermal and *in situ* synthesis methods, in which the comonomer was used as chemical bonding agent between the nanoparticles and the matrix, and acetylacetone (AcAc) was used as a size control agent of $ZrO_2$ in the PS matrix. Then, a new transparency film with a relatively high refractive index (1.72) was successfully obtained, in which $ZrO_2$ could be dispersed well in the PS–MPTMS matrix. Field emission scanning electron microscopy images indicated that AcAc was helpful in the dispersion of the nanoparticles, and smaller $ZrO_2$ particles with no aggregation were obtained in the PS–MPTMS matrix. The structure and thermal properties of the hybrid films were investigated by Fourier transform infrared spectroscopy and thermogravimetric analysis, and the surface properties were also examined. © 2013 Wiley Periodicals, Inc. J. Appl. Polym. Sci. 130: 2320–2327, 2013

**KEYWORDS:** functionalization of polymers; optical properties; polystyrene

Received 7 January 2013; accepted 11 April 2013; Published online 24 June 2013
**DOI: 10.1002/app.39403**

## INTRODUCTION

In the past years, optical materials have attracted much attention because they have many potential applications as photonic crystal films, optical waveguides, and antireflection films. Up to this point, many studies have been developed on the preparation and properties of hybrid materials; most of these hybrid materials contain nanoparticles because of their excellent optical properties, such as $TiO_2$,[1] ZnS,[2] and ZnO.[3] Recently, $ZrO_2$ nanomaterials have been received much attention because of their excellent abrasion resistance, flame retardance, and optical properties, and some hybrids have also been prepared with polystyrene (PS), poly(methyl methacrylate), and polycarbonate because theses polymers have good optical properties; for example, the refractive index of PS is as high as 1.59. So, a PS/$ZrO_2$ hybrid material will have potential applications, especially in the optical field.

In general, three strategies have been reported for the fabrication of thin films with high refractive indices with zirconia components: a filtered cathodic vacuum arc,[4] ion-beam-induced chemical vapor deposition,[5] and sputtering.[6] Some high refractive index hybrids with polar polymers as matrices have been prepared; epoxy-based, urethane-based,[7] acrylate-based,[8] and poly(vinylidene fluoride)[9] containing zirconia nanoparticles, for example, have been studied. However, few studies have focused on hybrids based on nonpolar polymers because of the quick hydrolysis and condensation process of zirconium(IV) *i*-propoxide and the poor compatibility between inorganic materials and polymers, for example, PS/$ZrO_2$, which may lead to difficulty in the control of the dispersion process of zirconia particles because of its self-aggregation. Aggregation will reduce the transparency of the hybrid films. In past years, many research efforts have been devoted to the stabilization and separation of nanoparticles by the capping of organic shells to overcome the inherent van der Waal's attraction between particles.[10–13] For example, Rao and Chen[14] obtained PS/$TiO_2$ nanocomposites by the *in situ* synthesis process to control the dispersion of $TiO_2$ in a polystyrene (PS)–γ-methacryloxypropyl trimethoxy silane (MPTMS) matrix (here, the addition of MPTMS comonomer could improve the interfacial reaction between PS and $TiO_2$), and the particles were controlled in the nanoscale. However, transparent PS–MPTMS/$ZrO_2$ hybrids are difficult to obtain because the zirconia precursor is more active.

To prepare polymer/$ZrO_2$ hybrid materials in which $ZrO_2$ is well dispersed in PS matrix, the hydrolysis and condensation of the zirconia precursor should be well controlled, and the interfacial effect between $ZrO_2$ and the polymer should be strong enough to prevent the $ZrO_2$ nanoparticles from aggregating. Therefore, PS–MPTMS should be prepared to improve the polarity of PS, and a stabilizer, such as acetylacetone (AcAc), is necessary to control the dispersion of $TiO_2$ in the polymer matrix. After that, the solution should be film-coated on Si wafers, and hybrid films can be prepared.[14]

**Table I.** Compositions of the PS–MPTMS/$ZrO_2$ Hybrid Materials

| | Zr0 | Zr20 | Zr40 | Zr60 | Zr80 | Zr100-0 | Zr100 |
|---|---|---|---|---|---|---|---|
| PS-MPTMS (g) | 1.25 | 1.25 | 1.25 | 1.25 | 1.25 | 1.25 | 1.25 |
| THF (g) | 23.75 | 23.75 | 23.75 | 23.75 | 23.75 | 23.75 | 23.75 |
| AcAc (g) | 0 | 0.25 | 0.5 | 0.75 | 1.00 | 0 | 1.25 |
| Zirconium(IV) *i*-propoxide (g) | 0 | 0.25 | 0.5 | 0.75 | 1.00 | 1.25 | 1.25 |

The solvothermal method is a general method for fabricating crystalline nanoparticles in the inorganic chemistry field,[15,16] and the reaction temperature is often set to lower than 200°C; this also fits the reaction for polymers. Because of the increased solubility and reactivity of the compounds and complexes under high temperatures and pressures, the solvothermal method can be used to synthesize copolymers that are difficult to obtain by traditional methods.[17–19] The organic functional groups under these circumstances are more reactive, and the polymerization process is easier to facilitate and more effective. On the other hand, the reaction time is also much shorter, and the solvent content is much lower than in solution polymerization. On the basis of the these reasons, transparent PS–MPTMS/$ZrO_2$ hybrid materials were successfully prepared by solvothermal and *in situ* composite synthesis methods. First, functionalized PS (PS–MPTMS) was synthesized by a solvothermal method. Second, the Zr precursor and AcAc were added to the PS–MPTMS solution, and hybrid films were prepared by an *in situ* composite synthesis method;[14] then, they were characterized by Fourier transform infrared (FTIR) spectroscopy, X-ray diffraction (XRD), and field emission scanning electron microscopy (FE-SEM). Finally, the optical, thermal, and surface energy properties of the PS–MPTMS/$ZrO_2$ hybrid materials were also studied.

## EXPERIMENTAL

### Materials

Zirconium (IV) *i*-propoxide (70 wt % solution in 1-propanol) was purchased from Aldrich Corp. (St. Louis, MO). γ-Methacryloxypropyl trimethoxy silane (MPTMS) was offered by GE Co. (A174, Fairfield, CT). Tetrahydrofuran (THF ≥99.0%), AcAc (≥99.0%), heptane (≥99.0%), 2,2-azobisisobutyronitrile (AIBN), and styrene (≥99.0%) were products of Sinopharm Chemical Reagent Corp. (Shanghai, China). Styrene was purified through vacuum distillation and finally kept at 2°C. AIBN was recrystallized before use. All solvents were used after they were dried with a molecule sieve.

### Synthesis of the PS–MPTMS Copolymer

The PS–MPTMS copolymer was synthesized by a solvothermal method. In a typical process, 2.84 g of MPTMS, 7.16 g of styrene, 0.05 g of AIBN, and 40 mL of THF were put into a 50-mL Teflon liner, and high-purity nitrogen was purged into the Teflon liner for 10 min to get rid of the oxygen. Then, the Teflon liner was slid into a stainless steel autoclave and sealed and put into a constant-temperature oven at a temperature of 160°C to carry out the reaction for 4 h. The copolymer precipitate was collected after the autoclave was cooled to room temperature, precipitated into 1 L of *n*-heptane, and then redissolved into 50 mL of THF; we then repeated the precipitation and filtration processes. Finally, the copolymer was washed with *n*-heptane several times and dried *in vacuo* to a constant weight, and the product yield was about 50 wt %.

### Preparation of the Zirconium(IV) *i*-Propoxide Containing Solution and Coatings

The as-synthesized PS–MPTMS copolymer (1.25 g) was dissolved in THF; then, AcAc was added to the solution with a syringe. Zirconium (IV) *i*-propoxide was then added to the previous solution, in which zirconium (IV) *i*-propoxide was kept from any hydrolysis and condensation. The composition is shown in Table I. The films were spin-coated on an Si wafer at a speed of 3500 rpm with a thickness of about 300 ± 50 nm. Then, the films were kept in a humidity oven and conditioned at 90% relative humidity and 70°C for 2 h. Finally, the films were treated at 60°C for 3 h and then at 150°C for 2 h.

### Characterization

FTIR spectroscopy was carried out on a Spectrum 100 instrument provided by PerkinElmer, Inc. (Waltham, MA). The wavelength was in the range 4000–400 $cm^{-1}$. The solution was dropped onto a KBr plate by a capillary first and dried under a high-voltage mercury lamp.

XRD was carried out on an XRD-6000 instrument (Shimadzu Co., Kyoto, Japan) in the temperature range 10–70°. The voltage and current of the X-ray tubes were 40 kV and 100 mA, respectively. The basal spacing of the montmorillonite was estimated from the position of the 001 peak in the XRD pattern.

FE-SEM was performed on a JSM-7401F instrument provided by JEOL, Ltd. (Tokyo, Japan). The surfaces of samples were dried under vacuum and then gold was evaporated before FE-SEM analysis.

Ultraviolet–visible spectra were measured on a UV-2450 spectrophotometer provided by Shimadzu Corp. The tests were undertaken in the range 400–900 nm.

Refractive index testing was carried out with an ellipsometer (NKD-8000, provided by Aquila Instruments, Ltd., Newport, United Kingdom). The refractive indices of the films were measured in the wavelength range 350–900 nm. The equipment was operated as follows: monochromatic light was focused onto the sample by a sophisticated beam-delivery device. The transmitted and reflected light were measured for p and s polarization. The light was measured with independent photodetectors. The data were collected, analyzed, and plotted with powerful Pro-Optix software. The software then used a variety of analytical models to represent the complex refractive indices of each material in the sample.

Thermogravimetric analyses (TGA) was determined by a TA Instruments TGAQ5000, which was provided by TA Instruments

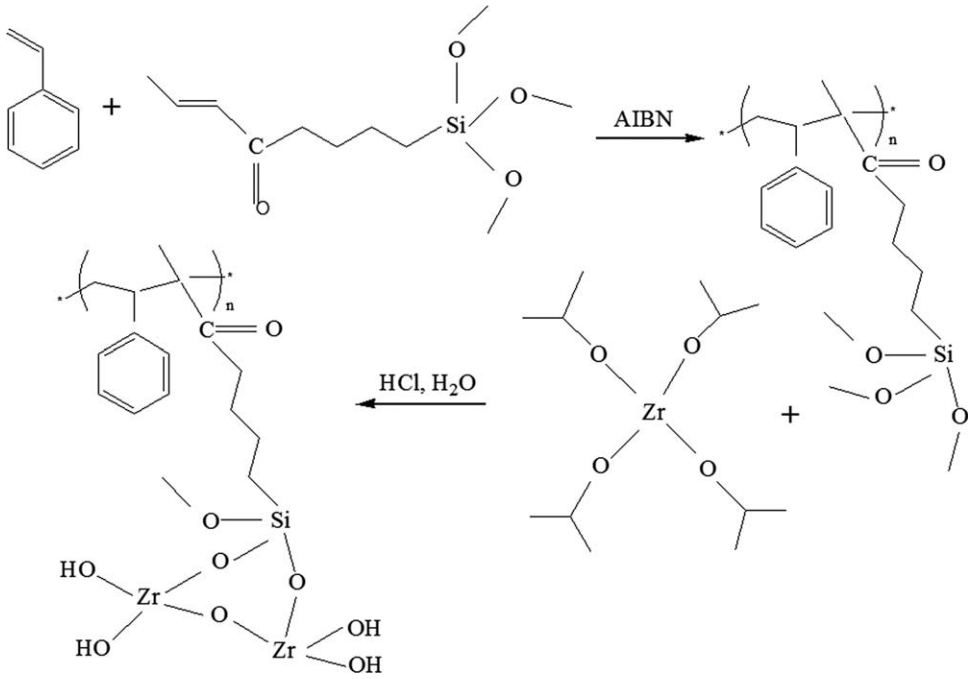


**Scheme 1.** Schematic diagram for the reaction among PS, MPTMS, and $ZrO_2$.

Co. (New Castle, DE). The tests were carried out under a nitrogen environment at a heating rate of 20°C/min in the range of room temperature to 700°C.

Contact angle measurements were tested with a OCA20 contact angle system provided by Dataphysics Corp. (San Jose, CA). The analyses were undertaken at room temperature by means of the sessile drop technique. Five measurements were performed on each sample, and the values were averaged. The measuring liquid was double-distilled water, and each drop contained about 3.5 mL of water.

## RESULTS AND DISCUSSION

### Preparation and Characterization of the PS–MPTMS/$ZrO_2$ Nanohybrid Materials

The sol–gel method is a general method for preparing hybrid materials, and the key factor of synthesizing a transparent and uniform hybrid solution is that the hydrolysis of the precursor should not be fast. If that condition is met, the synthesized nanoparticles aggregate easily. On this basis, it is difficult to synthesize hybrid materials with well-dispersed zirconia particles by this method. Therefore, it is also hard to synthesize hybrid materials with well-dispersed zirconia particles by the solvothermal method because of the faster hydrolysis process in high-temperature and high-pressure environments. Because of the special properties of the zirconia precursor, we chose the *in situ* method according to Rao and Chen,[14] and the chelant AcAc was also used to control the hydrolysis process of the zirconia precursor. Transparent hybrid films with a PS copolymer and zirconium(IV) *i*-propoxide were prepared. The samples were characterized by FTIR, XRD, and FE-SEM.

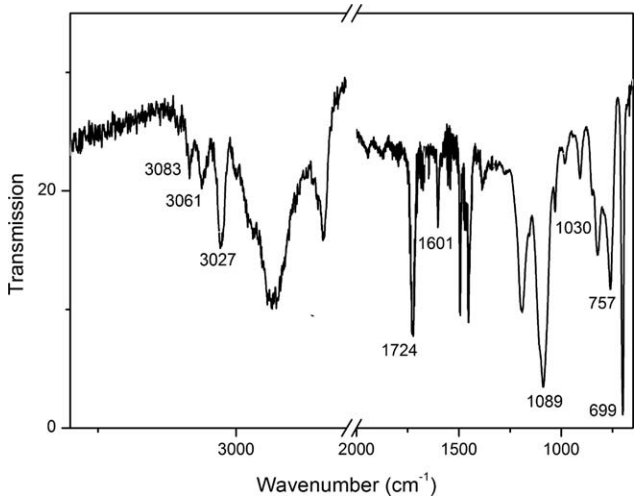


**Figure 1.** FTIR spectrum of sample Zr0 (PS–MPTMS).

To prepare transparent PS/$ZrO_2$ hybrids, the $ZrO_2$ particles should be well dispersed in the PS matrix. However, the polarity of $ZrO_2$ and the nonpolarity of PS make the dispersion and interfacial adhesion between them difficult; this leads to rather poor optical properties in the hybrids. Here, MPTMS as a comonomer was introduced onto the PS backbone to improve the interfacial adhesion. The reactions among PS, MPTMS, and $ZrO_2$ are described in Scheme 1.

The PS–MPTMS copolymer was first synthesized by a solvothermal method and was then purified. FTIR tests were undertaken with the purpose of proving the structure of the obtained copolymer, and the FTIR spectrum of the sample Zr0 (PS–MPTMS) film is shown in Figure 1.

As shown in Figure 1, the bands at 3083, 3061, and 3027 $cm^{-1}$ were the stretching vibrations of C—H on the benzene ring. The peaks at 757 and 699 $cm^{-1}$ were attributed to the in-plane stretching vibrations of C—H on the single-placed benzene ring. The band locked at 1601 $cm^{-1}$ was the framework vibration of

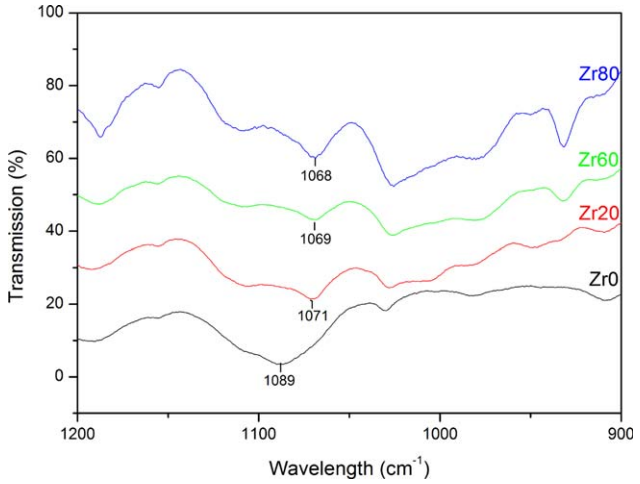


**Figure 2.** FTIR spectra of PS–MPTMS/$ZrO_2$ hybrids with different zirconia contents. [Color figure can be viewed in the online issue, which is available at wileyonlinelibrary.com.]

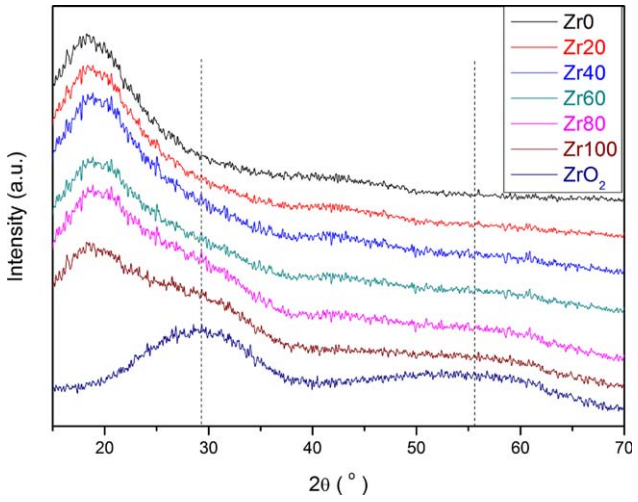


**Figure 3.** XRD patterns of the PS–MPTMS/$ZrO_2$ samples (a) Zr0, (b) $ZrO_2$, and (c) Zr40. [Color figure can be viewed in the online issue, which is available at wileyonlinelibrary.com.]

the benzene ring (ring breathing vibration). The band observed at 1724 $cm^{-1}$ was the characteristic peak of aliphatic ester. The peaks around 1089 and 1030 $cm^{-1}$ were the characteristic peaks of Si—O—Si. The previous analysis confirmed the existence of the MPTMS and styrene structure on Zr0; this indicated that the PS–MPTMS copolymer was successfully obtained by the solvothermal method.

Moreover, the influence of the amount of zirconia on the FTIR spectra is also discussed, and the results are shown in Figure 2. The peak at 1089 $cm^{-1}$, assigned to Si—O—Si, was observed, and it shifted gradually toward lower wave numbers with increasing content of $ZrO_2$. The shift of the Si—O band toward lower wave numbers was observed with $ZrO_2$,[20–24] $TiO_2$,[25] and $Al_2O_3$[26] because of the formation of Si—O—M heterolinkages (where M is second metal atom). So the shift of the band at 1089 to 1068 $cm^{-1}$ with increasing Zr content indicated a gradual increase in the Zr—O—Si population;[27] this indicated that the PS–MPTMS/$ZrO_2$ hybrid materials were prepared with different amounts of zirconia.

The XRD patterns of the PS–MPTMS, PS–MPTMS/$ZrO_2$, and pure $ZrO_2$ are shown in Figure 3. There were two broad peaks at 19 and 42° for PS–MPTMS due to the amorphous PS–MPTMS (black line), and the peaks at 29 and 56° for the pure $ZrO_2$ (navy line in the online figure) were attributed to the amorphous peaks of $ZrO_2$.[28] This indicated that the $ZrO_2$ prepared by the *in situ* method was an amorphous structure. Although for the PS–MPTMS/$ZrO_2$ composites (other color lines in the online figure), one peak appeared on the shoulder at 29°, and another peak appeared at 56° in addition to the peaks at 19 and 42°. The intensities of the 29 and 56° peaks increased with increasing zirconia contents and indicated that amorphous $ZrO_2$ particles existed in the PS–MPTMS/$ZrO_2$ composite, and the intensity of the peaks of $ZrO_2$ increased with increasing zirconia content. This also implied that the PS–MPTMS/$ZrO_2$ hybrids were obtained by solvothermal and *in situ* composite synthesis methods.

Because zirconium(IV) *i*-propoxide is more reactive, it is difficult to control the reaction temperature and humidity to obtain nanoparticles. Here, AcAc was used to control the hydrolysis and condensation of zirconium(IV) *i*-propoxide. FE-SEM images of the pure PS–MPTMS copolymer, PS–MPTMS/$ZrO_2$ without AcAc, and PS–MPTMS/$ZrO_2$ with AcAc are given in Figure 4. No nanoparticles were observed in the pure PS–MPTMS copolymer [Fig. 5(a)], whereas many particles with a large size distribution were observed in the PS–MPTMS/$ZrO_2$ hybrid without AcAc, and they were also dispersed in the matrix in a nonuniform manner [Fig. 5(b)]. With the addition of AcAc, more uniformed ZrO2 nanoparticles with sizes of 10–20 nm were uniformly dispersed in the PS matrix, and no agglomeration was observed in the PS–MPTMS/$ZrO_2$ hybrid [Fig. 5(c)]; this implied that AcAc was an effective dispersing agent that could effectively control the size of $ZrO_2$ in the PS–MPTMS matrix and prevent it from self-aggregating. The PS–MPTMS/$ZrO_2$ nanohybrid materials were successfully prepared because AcAc served as stabilizer for the zirconia precursor [$Zr(OCH_2CH_2CH_3)_4$] through a chelating process and further controlled the growth of $ZrO_2$ particles. The complexing reaction of the zirconium(IV) *i*-propoxide with AcAc at a molar ration of 1:1 is shown in Scheme 2.

### Properties of the PS–MPTMS/$ZrO_2$ Hybrid

The transmittance of the as-prepared PS–MPTMS/$ZrO_2$ nanohybrid materials in the ultraviolet–visible range is shown in Figure 5. More than 80% of the transmittance for the films indicated that the obtained hybrid films were transparent. The result was due to the fact that the particles dispersed in matrix were on the nanoscale and were well dispersed without aggregation; this was supported by theory.[29] From the Rayleigh scattering formula:

$$T = \frac{I}{I_0} = \exp\left\{-\frac{32\pi^4\Phi_p x r^3 n_m^4}{\lambda^4}\left[\frac{(n_p/n_m)^2-1}{(n_p/n_m)^2+2}\right]^2\right\} \quad (1)$$

where $I$ and $I_0$ are the intensities of the transmitted and incident light, respectively; $\lambda$ is the wavelength of light; $x$ is the

Applied Polymer SCIENCE

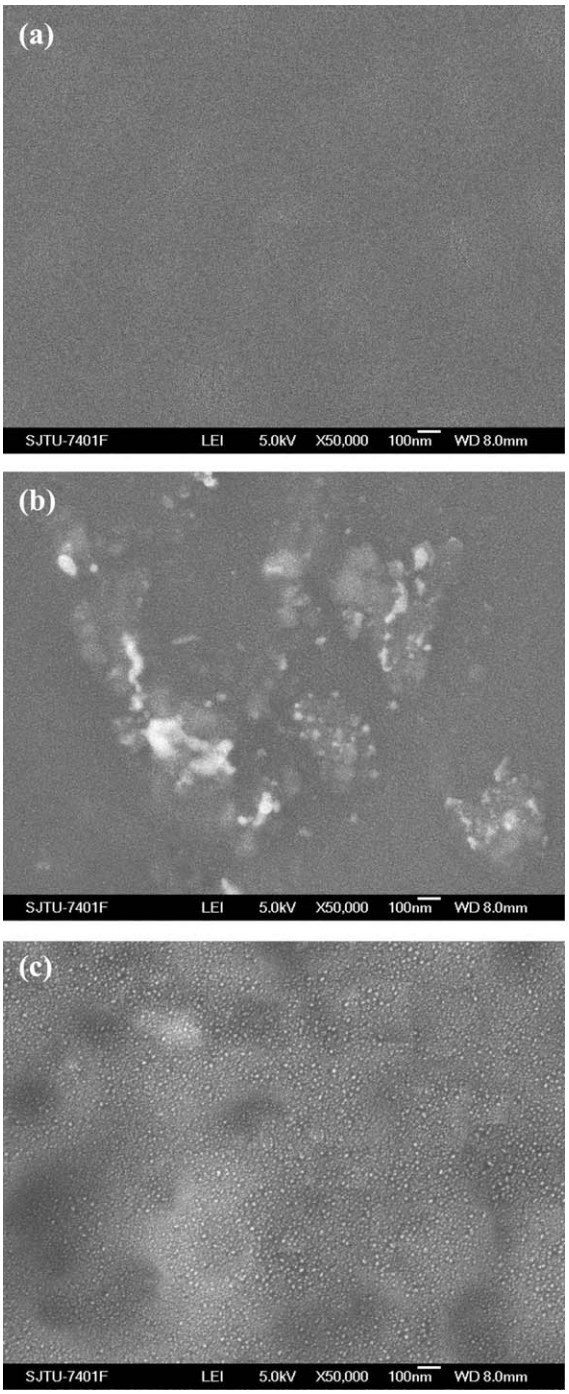


**Figure 4.** FE-SEM images of the hybrid nanocomposite films (a) Zr0, (b) Zr100-0, and (c) Zr100.

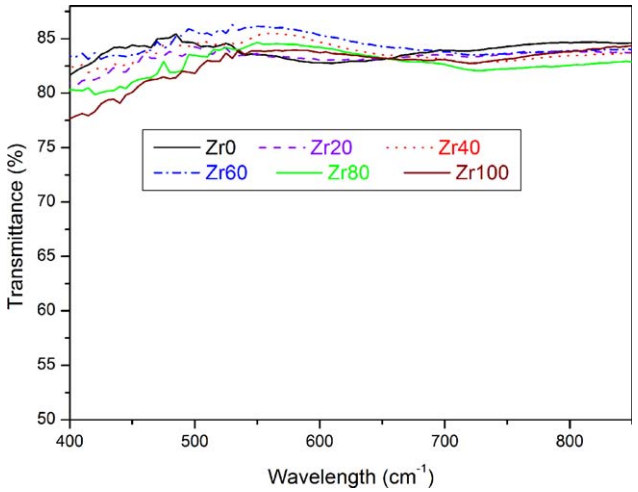


**Figure 5.** Transmittance of the hybrid films. [Color figure can be viewed in the online issue, which is available at wileyonlinelibrary.com.]

optical path length; and $n_p$ and $n_m$ are the refractive indices of the particles and the matrix, respectively.

In general, the inorganic domain size and the refractive index difference between the inorganic phase and matrix are believed to be the key factors influencing the transmittance of hybrid materials. The refractive index of the particles should be close to that of the matrix, or it will affect the transparency. On the other hand, decreasing the particle size can also improve the transparency of the nanocomposites because the optical scattering loss can be avoided when the inorganic domain size is less than one-tenth of the visible-light wavelength (200–800 nm); this implies that it is hard to retain the film transparency when highly inorganic particles are loaded. When more inorganic domains grow in the matrix, the nanoparticles will more easily aggregate, and this results in strong light scattering and low transparency in the visible region when the particles are larger than 100 nm, so particle sizes of 10 to 20 nm should be suitable.[29] The high transparency further confirmed that the PS–MPTMS/$ZrO_2$ hybrid films were nanodispersed. This result was in accordance with that of FE-SEM. The high transparency of films is an important index in many fields, including coatings and photoelectrical components. Also, low optical scattering is an important index for preparing high-refractive-index materials. Lenses with high transmittances and high refractive indices are studied extensively these days.

The refractive index of nano-$ZrO_2$ is relatively high compared to that of other inorganic particles. Increasing the content of nano-$ZrO_2$ in the PS–MPTMS matrix increased the refractive index of the hybrid materials, and the refractive index of the

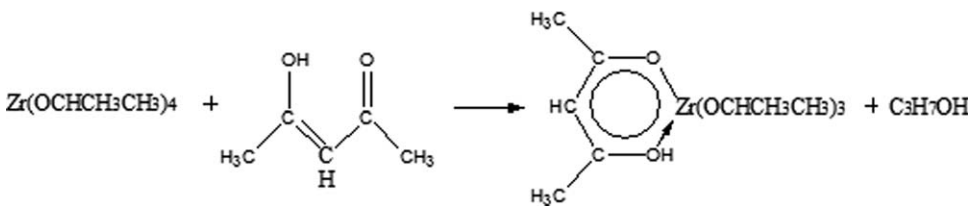


**Scheme 2.** Chelation between the zirconia precursor and AcAc.

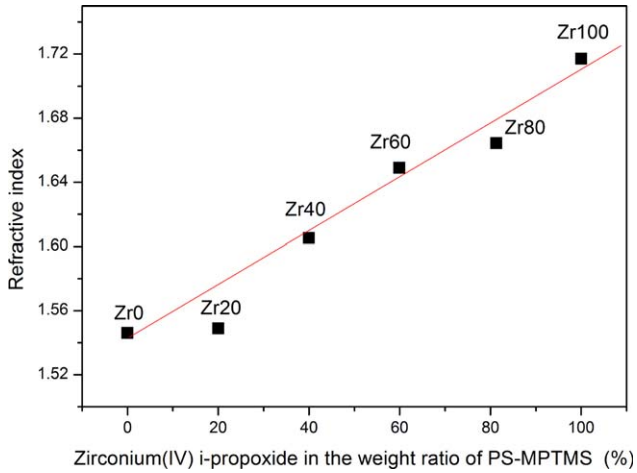


**Figure 6.** Variation in the refractive index of the PS–MPTMS/zirconia hybrid films with the zirconia content. [Color figure can be viewed in the online issue, which is available at wileyonlinelibrary.com.]

heterogeneous polymer could be computed by the Gladstone–Dale relation:

$$n=\sum_i v_i n_i \quad (2)$$

where $n_i$ and $v_i$ ($\Sigma v_i = 1$) are the refractive indices and volume fractions of the constituent phases of the components that make up the polymer.[30]

The effective refractive index ($n_{\text{eff}}$), calculated as a weighted volume fraction average ($f$) of the real refractive indices of the contributing media:[31]

$$n_{\text{eff}}=f_{\text{PS-MPTMS}}\times n_{\text{PS-MPTMS}}+(1-f_{\text{PS-MPTMS}})\times n_{ZrO_2} \quad (3)$$

where $n$ is the refractive index. As illustrated in the previous formulas, the refractive index and the content of inorganic nanoparticles in the matrix offer a great contribution to the refractive index of hybrid materials. Typical polymers have refractive indices between 1.40 and 1.67, and the refractive index of zirconia was 2.15–2.18. Therefore, more $ZrO_2$ nanoparticles in the PS–MPTMS matrix resulted in a higher refractive index. The refractive index of the hybrids with different contents of $ZrO_2$ is shown in Figure 6.

**Table II.** Char Yields of the Samples from the TGA Test

| | Zr0 | Zr20 | Zr40 | Zr60 | Zr80 | Zr100 |
|---|---|---|---|---|---|---|
| Char yield (wt %) | 7 | 14 | 16 | 19 | 21 | 22 |
| Yield at 250°C (wt %) | 99 | 96 | 95 | 94 | 94 | 93 |
| Yield at 350°C (wt %) | 58 | 83 | 81 | 79 | 79 | 79 |
| Yield at 475°C (wt %) | 12 | 23 | 24 | 26 | 27 | 27 |

As shown in Figure 6, the refractive index of the hybrid films increased along with the content of $ZrO_2$. The refractive index of the sample without any $ZrO_2$ was about 1.55. As the content of $ZrO_2$ increased, the refractive index increased step by step. The highest refractive index (Zr100) reached as high as 1.72. This tendency was in accordance with the theory.

To study the effect of $ZrO_2$ on the thermal properties of PS, the thermal properties of the as-prepared hybrid films were tested. The TGA curves and char yield are shown in Figure 7 and Table II.

As shown in Figure 7, there were three stages of weight loss. The first stage of weight loss was at 100–250°C. The second stage was around 350°C. The third stage was around 475°C. The first stage of weight loss was attributed to the loss of $H_2O$ bonded to the Si—O or Zr—O by hydrogen bonds. The first stage of weight loss was not obvious in the Zr0 sample because there was no Zr—O, only Si—O, so little $H_2O$ was bound.[32–34] The second stage of weight loss was attributed to the scission of

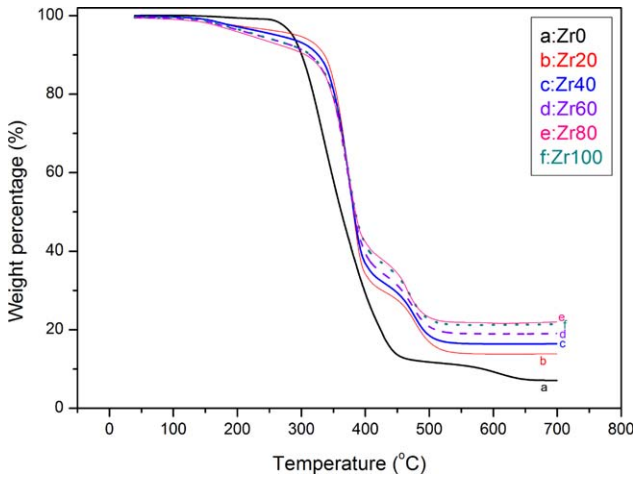


**Figure 7.** TGA curves of the hybrid materials. [Color figure can be viewed in the online issue, which is available at wileyonlinelibrary.com.]

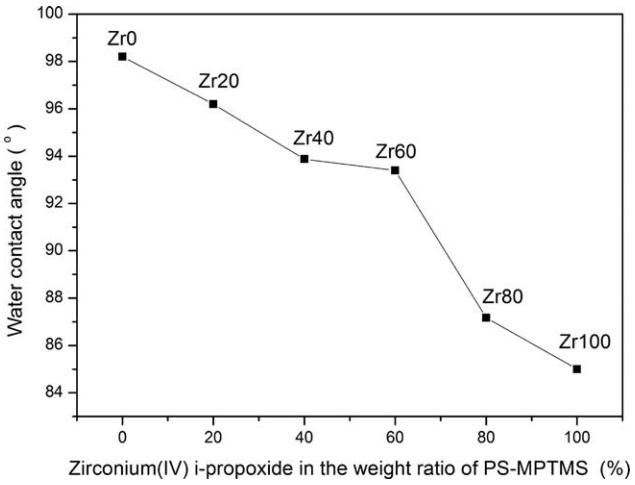


**Figure 8.** Water contact angle of the hybrid films versus the zirconia content.

phenyl groups and the random decomposition of the main chains. It was the main decomposition temperature of the polymer chain. When we compared the yield of samples Zr0 and Zr20 listed in Table II, we found that the yield (58 wt %) for Zr0 without any $ZrO_2$ was much lower than the yield (83 wt %) for Zr20 at 350°C; this indicated that $ZrO_2$ improved the thermal stability of the polymer chain; this was similar to the results of ref. 35. The third stage might have been due to the decomposition and dehydroxylation of the groups bonded to Si and Ti. From sample Zr0, there were still leftovers, which should have been $SiO_2$. The leftovers of the other samples were more than Zr0 because of $ZrO_2$ in the polymer matrix. As shown in Table II, the char yield for the samples increased with increasing zirconium(IV) *i*-propoxide content. Furthermore, it was obvious that the decomposition curves shifted to higher temperatures with increasing zirconia content from the last two stages; this indicated the enhancing effect of the thermal stability of the composite by the nanoparticles.

The surface energy of the hybrid films was an important property for the coating surface. The surface energy is usually evaluated by the water contact angle. The films were spin-coated on Si wafers, and their surface energies are shown in Figure 8.

As shown in Figure 8, the addition of nano-$ZrO_2$ led to a decrease in the water contact angle caused by the hydrophilicity of $ZrO_2$, and more $ZrO_2$ in the hybrid film led to a decrease in the water contact angle. So the addition of $ZrO_2$ nanoparticles changed the PS–MPTMS coating from hydrophobic to hydrophilic. Generally, some nanoparticles are hydrophilic in nature, such as $TiO_2$, $Al_2O_3$, and $ZrO_2$.[36] When more nanohydrophilic particles are added to the polymer matrix, the surface energy of the hybrid film get higher, and the water contact angle gets lower. In this way, the surface energy of coatings can be controllable by the addition of certain amounts of nanoparticles. So, coatings or films used in many special fields can be prepared by solvothermal and *in situ* composite synthesis methods.

## CONCLUSIONS

PS–MPTMS/$ZrO_2$ nanohybrid materials were successfully prepared by solvothermal and *in situ* composite synthesis methods, and their properties were investigated, including the optical and surface properties. The important results are as follows:

1. The $ZrO_2$ nanoparticles were well dispersed in the PS–MPTMS matrix; this confirmed the effectiveness of the functional comonomer MPTMS and stabilizer AcAc.
2. The as-prepared PS–MPTMS/$ZrO_2$ hybrid films had relatively high refractive indices (as high as 1.72) and high transmittance (ca. 80%).
3. The addition of $ZrO_2$ also improved the thermal stability of PS.
4. The decrease of the water contact angle of the hybrid films indicated that the addition of $ZrO_2$ changed the coatings from hydrophobic to hydrophilic.

## ACKNOWLEDGMENTS

The work described in this article was supported by the National Science Foundation of China (contract grant numbers 21173145 and 51133003) and Shanghai Leading Academic Discipline Project (contract grant number B202).

## REFERENCES

1. Mori, H.; Miyamura, Y.; Endo, T. *Mater. Chem. Phys.* **2009**, *115*, 287.
2. Lu, C. L.; Cui, Z. C.; Li, Z.; Yang, B.; Shen, J. C. J. *Mater. Chem.* **2003**, *13*, 526.
3. Tang, E. J.; Cheng, G. X.; Pang, X. S.; Ma, X. L.; Xing, F. B. *Colloid Polym. Sci.* **2006**, *284*, 422.
4. Zhao, Z. W.; Tay, B. K.; Huang, L.; Yu, G. Q. J. *Phys. D* **2004**, *37*, 1701.
5. Ferrer, F. J.; Frutos, F.; Garcia-Lopez, J.; Gonzalez-Elipe, A. R.; Yubero, F. *Thin Solid Films* **2007**, *516*, 481.
6. Zhao, S.; Ma, F.; Song, Z. X.; Xu, K. W. *Opt. Mater.* **2008**, *30*, 910.
7. Kudo, S.; Nagase, K.; Kubo, S.; Sugihara, O.; Nakagawa, M. *Jpn. J. Appl. Phys.* **2011**, *50*, 06GK12.
8. Omura, K.; Tomita, Y. J. *Appl. Phys.* **2010**, *107*, 023107.
9. Otsuka, T.; Chujo, Y. *Polymer* **2009**, *50*, 3174.
10. Murray, C. B.; Norris, D. J.; Bawendi, M. G. J. *Am. Chem. Soc.* **1993**, *115*, 8706.
11. Rockenberger, J.; Scher, E. C.; Alivisatos, A. P. J. *Am. Chem. Soc.* **1999**, *121*, 11595.
12. Balasubramanian, R.; Kwon, Y.-G.; Wei, A. J. *Mater. Chem.* **2007**, *17*, 105.
13. Physical Phenomena in Granular Materials; Geballe, T. H., Cody, G. C., Sheng, P., Eds.; MRS: Pittsburgh, **1990**; Vol. *195*, Chapter 1, p 1.
14. Rao, Y. Q.; Chen, S. *Macromolecules.* **2008**, *41*, 4838.
15. Du, W. M.; Qian, X. F.; Ma, X. D.; Gong, Q.; Cao, H. L.; Yin, H. *Chem.-Eur. J.* **2007**, *13*, 3241.
16. Zai, J. T.; Wang, K. X.; Su, Y. Z.; Qian, X. F.; Chen, J. S. J. *Power Sources* **2011**, *196*, 3650.
17. Gong, W. J.; Qi, R. R. J. *Appl. Polym. Sci.* **2009**, *113*, 1520.
18. Qi, R. R.; Liu, Q. C.; Wang, Y. L.; Huang, M. J. *Appl. Polym. Sci.* **2009**, *111*, 1069.
19. Shen, Y. H.; Qi, R. R.; Liu, Q. C.; Zhou, C. X. J. *Appl. Polym. Sci.* **2007**, *104*, 3443.
20. Miranda Salvado, I. M.; Serna, C. J.; Fernandez Navarro, J. M. J. *Non-Cryst. Solids* **1988**, *100*, 330.
21. Bosman, H. J. M.; Kruissink, E. C.; van der Spoel, J.; van den Brink, F. J. *Catal.* **1994**, *148*, 660.
22. Baudin, C.; Criado, E.; Bakali, J. J.; Pena, P. J. *Eur. Ceram. Soc.* **2011**, *31*, 697.
23. Zhang, Y.; Pan, L.; Gao, C. G.; Zhao, Y. X. J. *Sol–Gel Sci. Technol.* **2011**, *58*, 572.
24. Miller, J. B.; Rankin, S. E.; Ko, E. I. J. *Catal.* **1994**, *148*, 673.
25. Sohn, J. R.; Jang, H. J. J. *Catal.* **1991**, *132*, 563.

26. Miller, J. B.; Ko, E. I. *Catal. Today* **1997**, *35*, 269.

27. Zhan, Z.; Zeng, H. C. J. *Non-Cryst. Solids* **1999**, *243*, 26.

28. Ma, P.; Chen, S. L.; Hu, J. P.; Hu, J. C.; Duan, L. H.; Wang, Z.; Shao, J. D.; Fan, Z. X. *Acta Opt. Sinica* **2005**, *25*, 994.

29. Lü, C. L.; Yang, B. J. *Mater. Chem.* **2009**, *19*, 2884.

30. Polymer Handbook, 4th ed.; Brandrup, J., Immergut, E. H., Grulke, E. A., Abe, A., Bloch, D. R., Eds.; Wiley: New York, **1999**; Chapter VI, p 572.

31. Huang, K. J.; Rajendran, P.; Liddell, C. M. J. *Colloid Interface Sci.* **2007**, *308*, 112.

32. Han, Y. S.; Yamanaka, S. J. *Solid State Chem.* **2006**, *179*, 1146.

33. Yu, G.; Wang, X. Q.; Liu, J. R.; Xu, D. *Micropor. Mesopor. Mater.* **2010**, *130*, 189.

34. Aguilar, D. H.; Torres-Gonzalez, L. C.; Torres-Martinez, L. M.; Lopez, T.; Quintana, P. J. *Solid State Chem.* **2001**, *158*, 349.

35. Wang, H. T.; Xu, P.; Zhong, W.; Shen, L.; Du, Q. G. *Polym. Degrad. Stab.* **2005**, *87*, 319.

36. Feng, A. G.; McCoy, B. J.; Munir, Z. A.; Cagliostro, D. *Mater. Sci. Eng. A* **1998**, *242*, 50.